

DEPARTMENT OF BIOSYSTEMS SCIENCE AND ENGINEERING ETH ZÜRICH
INTRODUCTION TO BIOLOGICAL COMPUTERS
PROJECT REPORT

Design and *in-silico* modelling of a two input CRISPRi-based XNOR gate.

<i>Co-Author</i>	<i>Co-Author</i>	<i>Co-Author</i>	<i>Co-Author</i>
CHRISTOPHER WEINGARTEN	JAN NELIS	EMRE GÜRSOY	ANDREY CHERNOV
Student	Student	Student	Student
MSc Biology	MSc Biology	MSc Biology,	MSc Biology,
D-BSSE	D-BIOL	D-BSSE	D-BSSE
ETH Zürich	ETH Zürich,	ETH Zürich,	ETH Zürich
cweingar@ethz.ch	jnelis@ethz.ch	guersoye@ethz.ch	achernov@ethz.ch

Abstract: In recent years biological gates have first been applied to biomedical research and have shown to be promising tools to make next generation cell and gene therapies specific, safe, and effective. In this project, we design and simulate a CRISPRi-based XNOR gate *in-silico* with architecture based on a cascade of four universal NOR gates. The NOR gates are designed to receive dCAS9-KRAB RNPs as repressors and output sgRNAs, which then again assemble as a dCAS9-KRAB RNP to function as repressors in the downstream NOR gates. *In-silico* simulation of the XNOR gate is coherent with what would be expected for an XNOR gate. In the *in-silico* simulation we show that our system can generate a fold change in output of over 1000-fold. We further show that our system can be modified to function in alternative logics. We simulate and confirm the behaviour of a single NOR gate validating the system modularity. This validates our gate as effective and functional, considering our assumptions, to perform an XNOR logic, which was previously supported by *in-vivo* studies from literature.

ETH zürich



January 10, 2023

Introduction

The notion of computation and logic is often prescribed to digital systems, however living systems should not be omitted from the equation. Living organisms, including humans and single cells, have been observed to implement forms of complex computation, allowing them to modify their behaviour based on intra- and extracellular stimuli. An example would be cell differentiation based on decision-making signalling pathways during development (Sprinzak et al., 2010), or integration of neuronal signalling (McCulloch & Pitts, 1943).

Considering the existence of computation within living organisms, it is not unthinkable to link together our current understanding of mathematical computation, theory of electronics, and genetic engineering in order to modify cells to adapt their computational mechanisms for specific goals. In recent years, novel ideas such as bio-computing have been implemented, where cellular response mechanisms can be synthetically modified and novel molecular pathways introduced in order for cells to gain the capacity to perform actual computational algorithms (Lu, Khalil, & Collins, 2009; Grozinger et al., 2019).

In electronics, Boolean logic gates make up the foundation of computational algorithms, allowing the computer to perform calculations. The logic gate itself is a model of a Boolean function, a mathematical operation with one or multiple binary inputs, producing a binary output based on which algorithm is implemented. Taking an intrinsic capacity of cells to perform calculations based on signalling, these can be represented as a Boolean logic gate for simplification of understanding. This link between cellular processes and Boolean logic gates allows to synthesize new pathways, which upon introduction into cells will perform autonomous calculations (Weinberg et al., 2017; Miyamoto, Razavi, Derose, & Inoue, 2013).

We are now seeing a rapid development in the medical field towards first implementations of bio-computing in therapeutics (Angelici, Shen, Schreiber, Abraham, & Benenson, 2021; Liu et al., 2014). Nonetheless, translation of bio-computing approaches from theoretical models into *in-vitro* system and finally into *in-vivo* therapeutic strategies remains challenging. Similarly,

industrial processes are made more efficient, however remain wasteful and difficult to functionally optimize, but can be improved with synthetic logic circuits, for example using logic gates to control metabolic pathways, improving productions of bio-materials (He, Chen, Liang, & Qi, 2017). Still, synthetic logic gates for bio-computing are being thoroughly researched, and may serve as one of the stepping stones for advancements in multiple application fields.

Therefore, we have decided to develop a CRIPSRi-based biocomputational XNOR logic circuit, in order to contribute to the advancements in the field and provide ideas for potential use of this technology. The system architecture is chosen in a way so that the sensory module can be exchanged for an alternative sensory task. Furthermore, the system is composed entirely of universal NOR gates and can thus easily be modified to represent any logic gate desired.

XNOR-Gate

A negative exclusive NOR Gate, also called XNOR gate, is a logical gate and the logical component of a exclusive OR gate and is one of the sixteen possible logic gates of two input logical gates. In addition, it is a biconditional logical gate, meaning half of the Outputs are TRUE. It will only fall into TRUE statement if there neither or both inputs are present (Table 1).

Input I ₁	Input I ₂	Output
0	0	1
1	0	0
0	1	0
1	1	1

Table 1: Truth table of XNOR logic gate.

In electronics, a single XNOR logic gate can be used, whereas in a biological system there are no two-inputs XNOR gates known. In order to design an XNOR-Gate, a circuit of universal NOR-Gates was designed F1. The logical circuit consist of four NOR-Gates. In absence of inputs, the NOR-Gate 1 is permanently TRUE and thus set NOR-Gate 2 & 3 to FALSE, which results that NOR-Gate 4 is permanently activated. As soon as one Input is TRUE, either NOR Gate 2 & 3 switches to TRUE, which sets NOR Gate 4 to

FALSE. In presence of both Inputs, NOR-Gates 1,2 & 3 are FALSE causing a TRUE output from NOR gate 4. A detailed graphical simulation is shown in (supp F8)

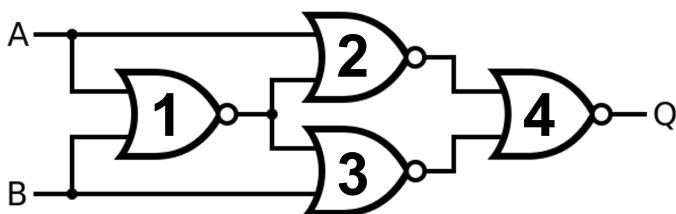


Figure F1: XNOR logic gate using four NOR gates, with inputs A and B and output Q.

CRISPRi

As the core of the project, we needed an efficient inhibitory system for the logic circuit to function. In order to ensure the outputs at each gate serve as inputs to the next within the circuit, we have settled with a fully RNA-based repression system, and thus have chosen the CRISPRi method of repression.

Catalytically deactivated "dead" Cas9 (dCas9) lacks its nuclease ability via point mutations in its HNH and RuvC domains, and thus does not introduce changes to the target DNA sequence (Qi et al., 2013). Transcription repression of the target gene can be realized through simple road block mechanics in the case of an RNP consisting of dCas9 and an sgRNA with respective target specificity.(Qi et al., 2013) To attain a more reliable mode of transcriptional repression dCas9 may be fused to a transcriptional repression domain such as the chromatin remodeling domain KRAB (Krüppel-associated box) which induces heterochromatin formation preventing transcription. (Alerasool, Segal, Lee, & Taipale, 2020) dCas9-KRAB fusion protein, guided by the guide RNA (gRNA), binds to a sequence (complementary to the gRNA) upstream of the PAM sequence, and by being fused to the chromatin effector domains of the KRAB protein, will silence the gene expression via repression at the promoter region. KRAB directs heterochromatin formation at the promoter by recruiting chromatin-modifying factors, compacting the chromatin and preventing access to the transcriptional machinery. (Alerasool et al., 2020)

CRISPR systems have numerous advantages, in

particular high precision, efficacy, and freedom of sequence targeting, since the targeting is done by guide RNA, which is encodable to any sequence. In particular this system, when fused to effector proteins, usually functioning as chromatin remodelers or direct inhibitors, the repression is more consistent and stronger (Lunge, Choudhary, Sharma, Gupta, & Agarwal, 2020).

However, one notable drawback of this set-up is, even though the system is reversible, the reversibility of the epigenetic repression caused by KRAB domain is slow. In such a scenario, reversing the switch to the other conformation will not be rapid, and thus the switch will not be rapid. Also possible toxicity due to constitutive expression of dCas9 may be questioned (Li et al., 2016). There may be other disadvantages related to the bulkiness of dCas9 protein, the requirement of transformation into the cell, PAM sequence requirement and possible effect on adjacent genes, however seeing as we are synthesizing plasmids to fit our circuit from scratch, this is less relevant for our set up (Lunge et al., 2020).

Feasibility

After developing the idea, the feasibility of the system must be critically evaluated. After researching the CRISPRi implementation in the synthetic XNOR circuits, two particular studies were found, that applied it. The first research paper was published by Martin Fussenegger of ETHZ-DBSSE and University of Basel, where they compiled complex logic circuits in human cells, applying CRISPR/Cas9 as the core processing unit. Despite the fact that they have not designed an XNOR circuit, their dCas9-KRAB system was effectively functional, being able to achieve 15-fold to 30-fold output repression for a single NOR gate (Kim, Bojar, & Fussenegger, 2019). The second paper was published by the Center of Synthetic Biology of Univeristy of Washington, in which they used dCas9-Mxi1 interference system to design six logic circuits for yeast cells. One of the circuits was an XNOR logic circuit with a set-up similar to our own (Figure F1), with which they were able to achieve a 10-fold output repression (Gander, Vrana, Voje, Carothers, & Klavins, 2017). These two studies reveal the practical application of our theoretical model, indicating its functional feasibility.

Methods

Host cells

A standard human cell line can be taken for expression and testing of the XNOR-gate, such as HEK293 cells. This cell line should also be compatible with the different components and regulatory sequences introduced in the following section.

Construct design

To achieve transcriptional repression, we are utilizing the CRISPR interference system (Qi et al., 2013; Mandegar et al., 2016). For our purpose we are expressing dCas9-KRAB from the eukaryotic EF1-a promoter, the dCas9-KRAB fusion contains an SV-40 NLS sequence and is proceeded by a beta-globin polyadenylation signal sequence. The dCAS9-NLS-KRAB sequences have been obtained from (Addgene plasmid # 110820) (Yeo et al., 2019). CRISPRi RNPs are targeted by sgRNAs to synthetic target sites preceding promoters driving target gene expression. The sgRNAs and their respective target sites have been designed with design principles for an optimal knockdown in mind. 20bp random DNA sequences starting with a G have been chosen as crRNA sequences. Random sequences have been generated via the Sequence Manipulation Suite (Stothard, 2000). All target sites possess a canonical NGG PAM sequence the gRNA scaffold has been obtained from Addgene plasmid #80036) (Doench & Root, 2016). Expression of crRNAs endogenously and sgRNAs in our case is best achieved by a polymerase III promoter. All sgRNAs are expressed from a human U6 promoter derived from the plasmid pLNHx_HsU6_shLuc (GenBank accession JN255690) (Duvoisin, Ayuk, Rinaldi, Suttiprapa, & Victoria, 2013). As inputs, the model receives two small molecules IPTG and aTC. IPTG binds LacI as an allosteric inhibitor, aTC binds TetR as an allosteric inhibitor. LacI and TetR are both expressed under an EF1-a promoter and are proceeded by a beta-globin polyadenylation signal sequence. The sequences for LacI and LacO have been derived from (Addgene plasmid # 158061) (Holden, Wickham, Webber, Thomson, & Trampari, 2020). The sequence for TetR has been derived from (Addgene plasmid # 22265) the se-

quence for a 7x TetO element has been obtained from (Addgene plasmid # 64238) (Shuen, Kan, Yu, Lung, & Lung, 2015). As a final output, the system has been designed to express GFP. GFP is expressed under the control of an EF1a Promoter and is proceeded by a beta-globin polyadenylation signal sequence. The GFP sequence has been obtained from (Addgene plasmid # 57822) (Stone et al., 2014).

The system is expressed from two expression plasmids. The expression plasmids contain an Ampicillin resistance gene as well an origin of replication for plasmid production in bacterial cells. The backbone for the two expression plasmids has been derived from (Addgene plasmid #55202). Each plasmid expresses a fluorescence marker to enable screening. On expression plasmid one (pBC001) mCerulean is expressed under the control of an EF1a Promoter and is proceeded by a beta-globin polyadenylation signal sequence. The mCerulean sequence has been derived from (Addgene plasmid #15214). On expression plasmid two (pBC002) mCherry is expressed under the control of an EF1a Promoter and is proceeded by a beta-globin polyadenylation signal sequence. The mCherry sequence has been derived from (Addgene plasmid #20956).

Full sequences can be found [online](#), sequence maps of the expression plasmids can be found in the appendix F11, F12.

System Design

The system is comprised of four individual NOR gates. The repressors utilized in all NOR gates are dCAS9-KRAB sgRNA RNPs whose target sites are upstream of each gates promoter driving the output. The general mechanism is that two RNPs generated either by the input layer or as an output of a NOR gate repress the output of the next downstream NOR gate. This yields a 4 NOR gate XNOR logic gate. The XNOR gate is comprised of 4 layers:

(A visualization of the below layout can be found in the appendix F10)

(1) The input sensing layer: The input sensing layer receives IPTG and aTC as small molecule inputs. IPTG is an allosteric repressor of LacI and aTC is an allosteric repressor of TetR. LacI and TetR are both parts of the first layer and are

expressed constitutively. LacI if not bound by IPTG binds to LacO which controls the transcription of sgRNA1; thus, in the presence of IPTG, LacO is free and sgRNA1 is expressed. This behaviour senses the presence or absence of input 1 which is IPTG. TetR if not bound by aTC binds to TetO, which controls the transcription of sgRNA2. Thus, in the same way, the LacI-IPTG system does, this senses the presence and absence of input 2, which is aTC. This input sensing layer encodes the inputs into sgRNAs, which can be received and used as digital inputs in the computation of the system.

(2) The initial layer: The initial layer is composed of a single NOR gate NOR1. NOR1 receives sgRNA1 and sgRNA2 as repressors expressed by the input sensing layer. NOR1 possesses two sgRNA target sites preceding its promoter, allowing each sgRNA1 and sgRNA2 to individually repress the output of NOR1. The output of NOR1 is sgRNA3.

(3) The transition layer: The transition layer is comprised of two NOR gates NOR2 and NOR3. NOR2 possesses two sgRNA target sites preceding its promoter, with both sgRNA1 and sgRNA3 individually repressing the output of NOR2. The output of NOR2 is sgRNA4. NOR3 again possesses two sgRNA target sites preceding its promoter, with both sgRNA2 and sgRNA3 individually repressing the output of NOR3. The output of NOR3 is sgRNA4 which is the same sgRNA as for NOR2.

(4) The output layer: The output layer is comprised of a single NOR gate NOR4. NOR4 performs a final computation and decodes the computed logic into a useful biologic output. NOR4 possesses one sgRNA target site for sgRNA4 preceding its promoter, as expressed by NOR2 and NOR3, repressing the output of NOR4. The output of NOR4 is GFP, which if not repressed by sgRNA4 is expressed from a constitutive promoter. GFP can then be sensed and quantified by e.g. fluorescence microscopy or flow cytometry to analyze and characterize the behaviour of the system.

As mentioned in the introduction we have created an XNOR gate based on universal NOR gates. Thus the logic of the system can be altered as desired based on the above-mentioned building blocks. The input sensing model can be exchanged entirely as long as it still drives the expression of sgRNA1 and sgRNA2. The final

output in this case GFP can be altered for any coding sequence desired ranging from alternative reporter genes to therapeutic proteins such as factor VIII or systems such as therapeutic CAR receptors. Detailed information on the individual component design can be found in the construct design section.

The system has been combined onto two expression plasmids, containing an antibiotic resistance for plasmid production in bacterial cells, as well as an origin of replication. Additionally, each plasmid contains a constitutively expressed fluorescence marker to be able to sort the double-positive population in a flow cytometer post-transfection. Therefore one should be able to select cells that have received both plasmids. Promoter cross-talk on the plasmids will most certainly be an issue and will need to be an object of optimization in the laboratory. To mitigate cross-talk one could use a set of each different u6 promoter as described in ([Adamson et al., 2016](#)). Nonetheless, the system will most certainly require optimization of the expression vectors to show the desired behaviour.

Model simulation

The reaction networks as well as ODE equations were generated on Simebio, an add-on of Matlab. For the simulations, ODE15 solver was used. The 3D input scans were simulated by using Matlab as well. All calculations and simulations were performed in Matlab environment.

Results

Requirements

We established two important requirements for the XNOR gate to be designed: Firstly, the XNOR gate needs to be functional in mammalian cells. Secondly, the output needs to be dynamic and reversible for targeted input detection. With these two conditions, detection of biomarkers and following actuation can be achieved in humans for biomedical application.

Assumptions & Calculations

All the concentration dependent parameters were converted to molecule/cell. Since the main net-

2

$$v = v_{max} \frac{(IC_{50})^n}{(IC_{50})^n + [Cas9 \cdot gRNA_x]^n} \cdot \frac{(IC_{50})^n}{(IC_{50})^n + [Cas9 \cdot gRNA_y]^n}$$

- Volume of a mammalian cell nucleus: $V_{cell} = 100 \mu\text{m}^3$ (Fujioka et al., 2006)
- Average Elongation rate of RNA Polymerase II & RNA Polymerase III: 6 nt/s (Darzacq et al., 2007). For simplification, average transcription rate for protein encoding transcription k_{mRNA} and average transcription rate for guide RNA k_{gRNA} were used:
 - $k_{mRNA} = 0.005 \text{ 1/s}$
 - $k_{gRNA} = 0.020 \text{ 1/s}$ ¹
- For transcriptional repression, Hill kinetic was used (Santillán, 2008). The hill equation with 2 repressor is described as :
 - $v_{max} = k_{transcription}[DNA]$
 - Hill coefficient n = 2.5 (Waterloo, 2022)
 - $IC_{50} = 16.8$ molecule (Waterloo, 2022), binding of Cas9-gRNA complex to target sequence
 - TetR/LacI: $IC_{50} = 60.22$ molecule
- Average translation rate based on in mammalian cell culture $k_{translation} = 0.015 \text{ 1/s}$ (Ingolia, Lareau, & Weissman, 2011)
- All mRNA as well as gRNA degradation rates are equal (ignoring length of mRNA/gRNA, modifications and secondary structure). Average half-life of a mRNA: $t_{1/2mRNA} = 50 \text{ min}$. Degradation as first-order reaction. Thus $k_{deg_{mRNA}} = 2.3 * 10^{-4} \text{ 1/s}$ (Björn et al., 2016)
- All protein degradation rates are equal (ignoring protein structure and stability). Degradation rate based on the average

work only reacted within the nucleus, the reaction volume V_{cell} is the volume of the cell nucleus.

protein half-life in mammalian cells (7 hours)(Eran et al., 2011). $k_{deg_{protein}} = 2.75 * 10^{-5} \text{ 1/s}$

- Binding of IPTG/aTC to LacI/TetR k_{on} IPTG/aTC + LacI/TetR = $1.66 * 10^{-4}$ (Stamatakis & Mantzaris, 2009)
- Disassociation of IPTG/aTC to LacI/TetR k_{off} IPTG/aTC + LacI/TetR = $1.93 * 10^{-4}$ (Stamatakis & Mantzaris, 2009)
- Binding of guide-RNA to Cas9 k_{on} gRNA + Cas9 = $1.66 * 10^{-5} \text{ 1/(molecule*second)}$ (Huang, Seeger, Danielson, & Lindblad, 2015)
- Disassociation of guide-RNA to Cas9 k_{off} gRNA + Cas9 = 10^{-5} 1/second (Huang et al., 2015)
- gRNA can not be degraded when in complex with the dCas9 and is degraded along with the protein part of the complex.
- There is no non-specific binding.
- Parameters for dCas9-KRAB fusion are the same as for Cas9.
- dCas9-KRAB repression functions at a 100% rate.
- dCas9-KRAB repression is fully and quickly reversible.
- Maturation time of the fluorescence reporters is not considered, for simplification purposes.

¹For production of guide-RNA a first-order reaction was assumed. However, since no parameter were found, we estimated a value between the average transcription rate k_{mRNA} and the theoretical maximum transcription rate $k_{gRNA_{max}} = 0.06 \text{ 1/s}$

Model Results

NOR-Gate

Since the XNOR-Gate is based on four individual NOR-Gates, the robustness of a single NOR Gate is essential for the system. A simulation of NOR-Gate 4 was carried out to show the sensitivity at different gRNA 3 and 4 concentrations (see figure F2). GFP concentration was at approx. 12000 molecules/cell at Cas9-gRNA complex concentration from 0-8 molecules/cell. After 8 molecules/cell the GFP concentration decreased.

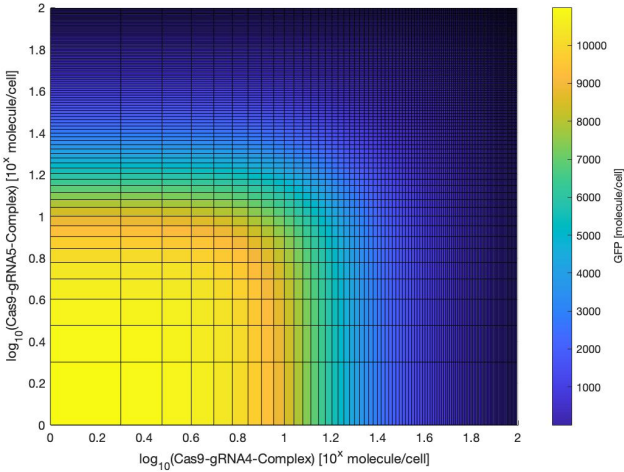


Figure F2: GFP values at steady state shown as color gradient as a function of gRNA4- gRNA5-complex.

XNOR-Gate

The simulation was carried out scanning different input concentration over four orders of magnitude, resulting in figure F3. We can see that the model does indeed act as an XNOR-gate, expressing high levels of GFP at low and high concentrations of both inputs, while GFP levels drop drastically when only one input is expressed highly. GFP levels for a positive output is 1880 molecules/cell, dropping to 15 molecules/cell for the negative output, showing us we have about a 100-fold change in GFP signal.

The transition form high to low GFP expression happens between 10^2 and 10^3 molecules of input. To further characterize this these transition phases, we again scanned over that range with smaller step sizes, the results of which can be seen in figure F4. Here we can see the transition

follows a steep sigmoidal curve as expected from the Hill inhibition kinetics.

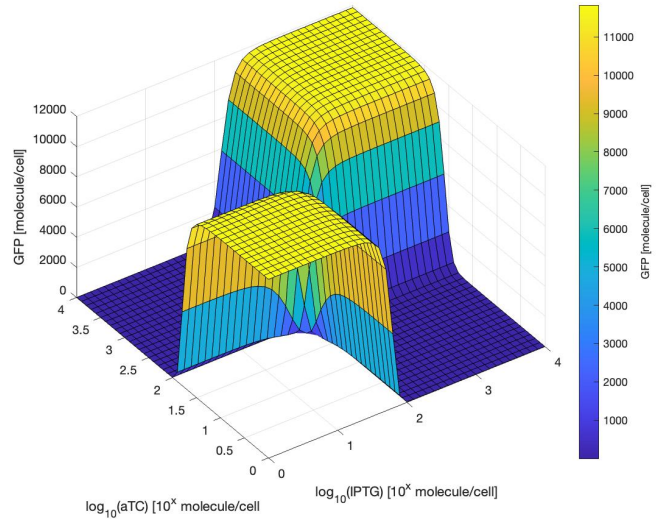


Figure F3: GFP levels as a function of the two inputs aTc IPTG. GFP levels were scanned over input levels of four orders of magnitude ($10^0 - 10^4$ molecule/cell) with step size $10^{0.1}$ and visualized in a surface plot.

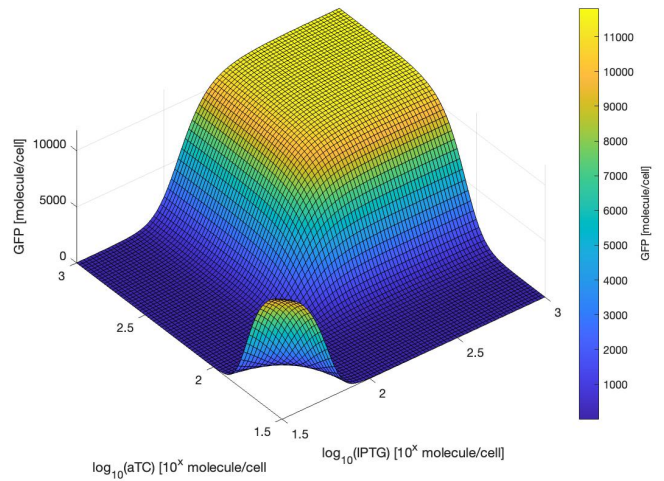


Figure F4: GFP levels as a function of the two inputs aTc IPTG. To further characterize the transition phases, GFP levels were scanned between input levels of $10^{1.5}$ and 10^3 with step size $10^{0.02}$ and again visualized in a surface plot.

To further investigate the behavior of the model, we ran the model for each of the four different model outputs and looked at the levels of the five different gRNA-Cas9 complexes. As can be seen in figure F5, the expression complexes follows our expectations from the theoretical XNOR gate in

figure F1. For condition 0/0 (representing the two input levels in molecules/cell), we can see that only the gRNA3 complex is formed, inhibiting both the GFP-inhibiting gRNAs and allowing for GFP expression. For condition 0/1000 and 1000/0, we can see that both the respective input-gRNA and GFP-inhibiting gRNA complex are expressed, reducing GFP expression. For the final condition, 1000/1000, both the input-gRNA complexes are expressed, which together inhibit both GFP-inhibiting gRNA complexes, again giving us high GFP levels.

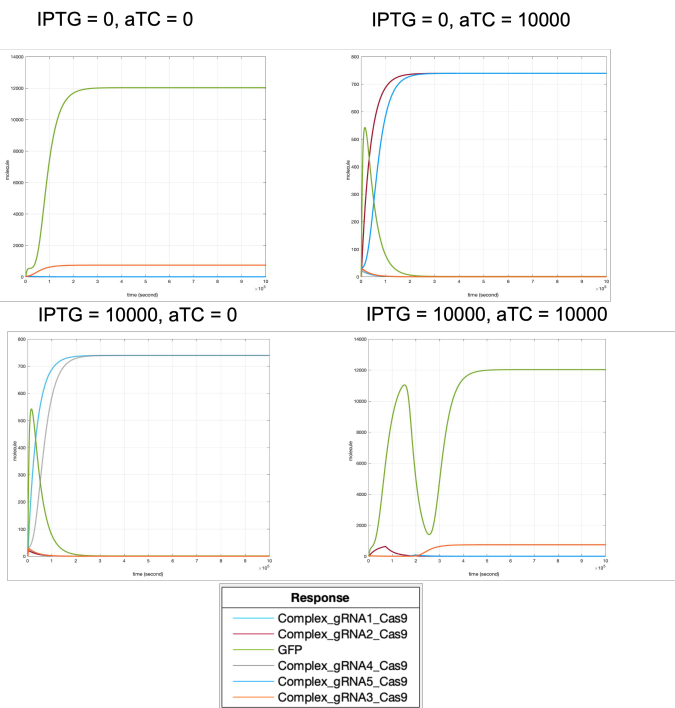


Figure F5: GFP gRNA complex levels in two plots for each of the four different conditions in the truth table (Table 1).

Parameter Scan

To get a better feeling of how the model would act if we use a weaker repressor, we did a parameter scan for the Cas9 dissociation constant. We scanned over four orders of magnitude and observed how the reliance of GFP on a single input level changes.

From figure F6, we can see that the required input levels increase with increasing K_d , behaving as expected. At K_d values over 100, however, the fold-change of GFP starts to drop drastically, ultimately not showing any repression at all at high levels of single input. The general drop in GFP levels at higher K_d s could be attributed to the simulation not reaching steady state with the

given time.

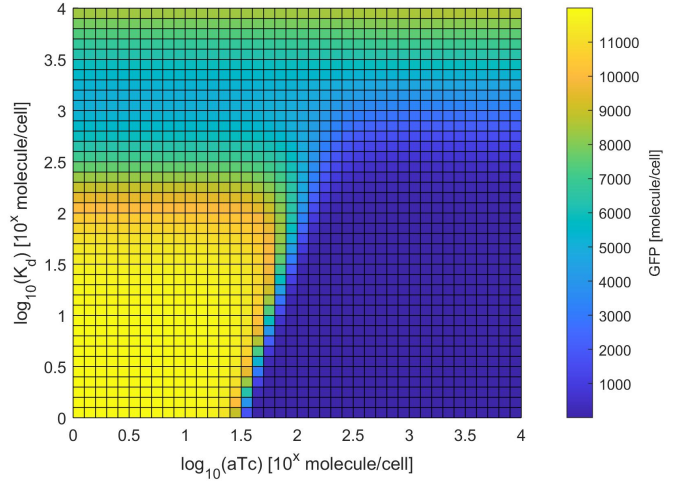


Figure F6: Parameter scan for the dissociation constant K_d of the gRNA-Cas9 complex to its DNA substrate. For each K_d , the reliance of GFP on a single input (aTc; IPTG is permanently set to zero) can be observed. The behaviour above the K_d of 2.5 could be explained by the system not reaching the steady state during the simulation.

Discussion

Model Performance

As seen in the results, the model follows the expected XNOR logic, and has a 1000-fold difference in output. From the parameter scan we can however see that the circuit can quickly break down if affinity and repression isn't strong enough. Considering the much lower fold-change described in Fussenegger's paper, which was around 15-30 fold for a single NOR gate (Kim et al., 2019), it is likely that we chose a very optimistic affinity parameter in idealized conditions. It also, however, shows that there is a significant fold change and the gate could be viable in an experimental setting.

Flexibility and Scalability

The designed XNOR gate has several advantages when considering flexibility. The inputs can be freely exchanged for specific needs, as long as the input can influence transcription rates of DNA. Though there might be some problems us-

ing miRNA as inputs, since these do not target gRNAs efficiently, this could also be solved by designing a repressor of the two primary gRNAs which could be targeted by miRNAs. The output can also be chosen freely, and is not limited to proteins, but could also express miRNAs or another gRNA for regulating specific pathways. Additionally, by simply adding another NOT gate, e.g. by replacing the GFP with an miRNA which then targets the mRNA of the output protein component (Rinaudo et al., 2007), this gate can easily be reprogrammed to follow an XOR logic without greatly decreasing input to output speed.

The circuit is however not largely scalable. One advantage is the energy consumption; while the energy consumption is not low due to the requirement of constitutive synthesis of dCas9-KRAB, the gRNA components which are required to create additional gates do not have a very high energy cost. Therefore adding a second XNOR module in a cell would not require much more energy than only having one module.

The factor which is more likely to limit scalability is the size of the module; even with just a single XNOR gate, we would likely need two plasmids to implement the system, assuming the different circuit elements would not suffer from crosstalk. This could quickly limit what is practically viable and easily applicable.

Application

While the XNOR gate designed here has no specific application in mind, the development of a diverse range of gate logics and mechanisms is essential for the exploitation of different markers found in various diseases, especially cancer. This is also why the requirement for the circuit to work in mammalian cells was established from the start.

There are however very little examples where an XNOR or XOR gate is useful in biological or medical applications. One example found which follows an XNOR logic is the secretion of IgM in human primary B cells, which relies on the correct level of lymphocyte-specific protein tyrosine kinase (LCK) in a bandpass-like regulation. LCK in turn is controlled by both an inhibitor and an activator. In the presence of solely the inhibitor or the activator, LCK levels are too low or too

high, respectively, and IgM secretion is inhibited. When however both or neither are present, required LCK levels are restored and IgM is secreted (Zhou, Zhang, Henriquez, Crawford, & Kaminski, 2018).

By aiming to sense the activator and inhibitor with an XNOR gate, it could be more reliable and more specific than solely measuring the presence of IgM or LCK. Additionally, creating a gate for a bandpass-like input such as the LCK levels in the human primary B cells can be challenging, making an XNOR gate with two "binary" inputs more attractive.

Finally, by exploiting the fact that an XOR gate only requires an additional NOT gate at the end of the XNOR module, and using the half adder system designed in Martin Fussengger's paper (Kim et al., 2019), a full adder circuit could theoretically be designed. Considering the number of gates and components needed, this would, however, be quite an ambitious project.

Caveats

The system presented here requires reversible and dynamic repression, which we have decided to simulate using a dCas9-KRAB complex. This complex inhibits expression by i) sterically blocking RNA-Polymerase association (Qi et al., 2013), and ii) inducing heterochromatin formation through histone methylation and deacetylation (Yeo et al., 2019). While both of these processes have been shown to be reversible (Groner et al., 2012), histone methylation and deacetylation, as well as heterochromatin formation, are not necessarily quickly reversible. Thus the assumption that strong expression proceeds as soon as the dCas9-KRAB complex is no longer associated to the respective promoter does not necessarily hold true. This could be solved by using a weaker but more quickly reversible repressor than the KRAB domain or solely relying on the steric repression of dCas9. This would however be a trade-off between reversibility and repression strength, risking higher leakiness. These different possibilities would have to be tested experimentally before application in a larger circuit such as our XNOR gate.

Another difficulty with the circuit is the large amount of components to implement a single logic gate, as already mentioned in the scalability sec-

tion. The delivery vector would need to be optimized and condensed as much as possible while avoiding crosstalk, which might be challenging and require a great amount of experimental work.

Conclusion

Implementing logical function into a cell allows for *in-situ* bio computation and allow for autonomous decision making of the cell. While we were successful in achieving a dynamic range of over 1000-fold, our model turned out to be

overoptimistic, as numerous potential modifications should be implemented to improve the model, such as introducing a leakage term into the Hill equation, among others. Whereas AND and NOR Gates were already implemented, the application of an XNOR-Gate shows that these modules can be combined and used to create different logic gates which are not easily achievable in biological systems. While the direct applications for an XNOR gate is limited in a biomedical setting, the ability to choose from a wide array of tools and logic gates is important for quickly exploiting new findings and targeting diseases.

References

- Adamson, B., Norman, T. M., Jost, M., Cho, M. Y., Nuñez, J. K., Chen, Y., ... Weissman, J. S. (2016). A Multiplexed Single-Cell CRISPR Screening Platform Enables Systematic Dissection of the Unfolded Protein Response. *Cell*, *167*(7), 1867–1882. doi: 10.1016/j.cell.2016.11.048
- Alerasool, N., Segal, D., Lee, H., & Taipale, M. (2020). An efficient KRAB domain for CRISPRi applications in human cells. *Nature Methods*, *17*(11), 1093–1096. Retrieved from <http://dx.doi.org/10.1038/s41592-020-0966-x> doi: 10.1038/s41592-020-0966-x
- Angelici, B., Shen, L., Schreiber, J., Abraham, A., & Benenson, Y. (2021, 12). An AAV gene therapy computes over multiple cellular inputs to enable precise targeting of multifocal hepatocellular carcinoma in mice. *Science Translational Medicine*, *13*(624). Retrieved from <https://www.science.org/doi/10.1126/scitranslmed.abh4456> doi: 10.1126/scitranslmed.abh4456
- Björn, S., Margaux, M., Benedikt, Z., Katja, F., Carina, D., Achim, T., ... Patrick, C. (2016, 6). TT-seq maps the human transient transcriptome. *Science*, *352*(6290), 1225–1228. Retrieved from <https://doi.org/10.1126/science.aad9841> doi: 10.1126/science.aad9841
- Darzacq, X., Shav-Tal, Y., De Turris, V., Brody, Y., Shenoy, S. M., Phair, R. D., & Singer, R. H. (2007). In vivo dynamics of RNA polymerase II transcription. *NATURE STRUCTURAL & MOLECULAR BIOLOGY*, *14*. Retrieved from <http://www.nature.com/nsmb> doi: 10.1038/nsmb1280
- Doench, J., & Root, D. (2016). Optimized sgRNA design to maximize activity and minimize off-target effects of CRISPR-Cas9 Synthesis of an arrayed sgRNA library targeting the human genome. *Nature Biotechnology*, *34*(2), 184–191. Retrieved from <https://www.ncbi.nlm.nih.gov/pmc/articles/PMC4744125/pdf/nihms-740733.pdf> doi: 10.1038/nbt.3437.Optimized
- Duvoisin, R., Ayuk, M. A., Rinaldi, G., Suttiprapa, S., & Victoria, H. (2013). Human U6 promoter drives stronger shRNA activity than its schistosome orthologue in Schistosoma mansoni and human fibrosarcoma cells. , *21*(3), 511–521. Retrieved from <https://www.ncbi.nlm.nih.gov/pmc/articles/PMC3271131/pdf/nihms328517.pdf> doi: 10.1007/s11248-011-9548-0.Human
- Eran, E., Naama, G.-Z., Irina, I., Ariel, C., Erez, D., Tamar, D., ... Uri, A. (2011, 2). Proteome Half-Life Dynamics in Living Human Cells. *Science*, *331*(6018), 764–768. Retrieved from <https://doi.org/10.1126/science.1199784> doi: 10.1126/science.1199784
- Fujioka, A., Terai, K., Itoh, R. E., Aoki, K., Nakamura, T., Kuroda, S., ... Matsuda, M. (2006, 3). Dynamics of the ras/erk mapk cascade as monitored by fluorescent probes. *Journal of Biological Chemistry*, *281*, 8917-8926. Retrieved from <https://pubmed.ncbi.nlm.nih.gov/16418172/> doi: 10.1074/jbc.M509344200
- Gander, M. W., Vrana, J. D., Voje, W. E., Carothers, J. M., & Klavins, E. (2017). Digital logic circuits in yeast with CRISPR-dCas9 NOR gates. *Nature Communications*, *8*(May), 1–11. Retrieved from <http://dx.doi.org/10.1038/ncomms15459> doi: 10.1038/ncomms15459
- Groner, A. C., Tschopp, P., Challet, L., Dietrich, J.-E., Verp, S., Offner, S., ... Trono, D. (2012, 7). The Krüppel-associated Box Repressor Domain Can Induce Reversible Heterochromatization of a Mouse Locus in Vivo. *Journal of Biological Chemistry*, *287*(30), 25361–25369. Retrieved from [https://www.jbc.org/article/S0021-9258\(20\)73701-4/fulltext](https://www.jbc.org/article/S0021-9258(20)73701-4/fulltext) doi: 10.1074/jbc.M112.350884
- Grozinger, L., Amos, M., Gorochowski, T. E., Carbonell, P., Oyarzún, D. A., Stoof, R., ... Goñi-Moreno, A. (2019, 12). Pathways to cellular supremacy in biocomputing. *Nature Communications*, *10*(1). Retrieved from <https://www.nature.com/articles/s41467-019-13232-z> doi: 10.1038/s41467-019-13232-z
- He, X., Chen, Y., Liang, Q., & Qi, Q. (2017, 3). Autoinduced AND Gate Controls Metabolic Pathway Dynamically in Response to Microbial Communities and Cell Physiological State. *ACS Synthetic Biology*, *6*(3), 463–470. Retrieved from <https://pubs.acs.org/doi/10.1021/acssynbio.6b00177> doi: 10.1021/acssynbio.6b00177
- Holden, E. R., Wickham, G. J., Webber, M. A., Thomson, N. M., & Trampari, E. (2020). Donor plasmids for phenotypically neutral chromosomal gene insertions in Enterobacteriaceae. *Mi-*

- crobiology (United Kingdom)*, 166(12), 1115–1120. doi: 10.1099/mic.0.000994
- Huang, H.-H., Seeger, C., Danielson, U. H., & Lindblad, P. (2015). Analysis of the leakage of gene repression by an artificial TetR-regulated promoter in cyanobacteria. *BMC Res Notes*, 8, 459. doi: 10.1186/s13104-015-1425-0
- Ingolia, N. T., Lareau, L. F., & Weissman, J. S. (2011). Ribosome profiling of mouse embryonic stem cells reveals the complexity and dynamics of mammalian proteomes. *Cell*, 147(4), 789–802. Retrieved from <http://dx.doi.org/10.1016/j.cell.2011.10.002> doi: 10.1016/j.cell.2011.10.002
- Kim, H., Bojar, D., & Fussenegger, M. (2019, 4). A CRISPR/Cas9-based central processing unit to program complex logic computation in human cells. *Proceedings of the National Academy of Sciences*, 116(15), 7214–7219. Retrieved from <https://www.pnas.org/content/116/15/7214> doi: 10.1073/pnas.1821740116
- Li, X. T., Jun, Y., Erickstad, M. J., Brown, S. D., Parks, A., Court, D. L., & Jun, S. (2016, 12). TCRISPRi: Tunable and reversible, one-step control of gene expression. *Scientific Reports*, 6. Retrieved from <https://www.nature.com/articles/srep39076> doi: 10.1038/srep39076
- Liu, Y., Zeng, Y., Liu, L., Zhuang, C., Fu, X., Huang, W., & Cai, Z. (2014). Synthesizing and gate genetic circuits based on CRISPR-Cas9 for identification of bladder cancer cells. *Nature Communications*, 5. Retrieved from <https://www.nature.com/articles/ncomms6393> doi: 10.1038/ncomms6393
- Lu, T. K., Khalil, A. S., & Collins, J. J. (2009). Next-generation synthetic gene networks. *Nature Biotechnology*. Retrieved from <https://www.nature.com/articles/nbt.1591> doi: 10.1038/nbt1591
- Lunge, A., Choudhary, E., Sharma, R., Gupta, R., & Agarwal, N. (2020). Functional understanding of CRISPR interference: its advantages and limitations for gene silencing in bacteria. In *Genome engineering via crispr-cas9 system* (pp. 199–218). Elsevier. Retrieved from <https://www.sciencedirect.com/science/article/pii/B9780128181409000179> doi: 10.1016/b978-0-12-818140-9.00017-9
- Mandegar, M. A., Huebsch, N., Frolov, E. B., Shin, E., Truong, A., Olvera, M. P., ... Conklin, B. R. (2016). CRISPR Interference Efficiently Induces Specific and Reversible Gene Silencing in Human iPSCs. *Cell Stem Cell*, 18(4), 541–553. Retrieved from <http://dx.doi.org/10.1016/j.stem.2016.01.022> doi: 10.1016/j.stem.2016.01.022
- McCulloch, W. S., & Pitts, W. (1943). *A LOGICAL CALCULUS OF THE IDEAS IMMANENT IN NERVOUS ACTIVITY* (Vol. 5; Tech. Rep.). Retrieved from <https://link.springer.com/article/10.1007/BF02478259> doi: <https://doi.org/10.1007/BF02478259>
- Miyamoto, T., Razavi, S., Derose, R., & Inoue, T. (2013, 2). *Synthesizing biomolecule-based boolean logic gates* (Vol. 2) (No. 2). Retrieved from <https://pubs.acs.org/doi/10.1021/sb3001112> doi: 10.1021/sb3001112
- Qi, L. S., Larson, M. H., Gilbert, L. A., Doudna, J. A., Weissman, J. S., Arkin, A. P., & Lim, W. A. (2013). Repurposing CRISPR as an RNA-guided platform for sequence-specific control of gene expression. *Cell*, 152(5), 1173–1183. Retrieved from <http://dx.doi.org/10.1016/j.cell.2013.02.022> doi: 10.1016/j.cell.2013.02.022
- Rinaudo, K., Bleris, L., Maddamsetti, R., Subramanian, S., Weiss, R., & Benenson, Y. (2007, 7). A universal RNAi-based logic evaluator that operates in mammalian cells. *Nature Biotechnology*, 25(7), 795–801. Retrieved from <https://www.nature.com/articles/nbt1307#citeas> doi: 10.1038/nbt1307
- Santillán, M. (2008). On the Use of the Hill Functions in Mathematical Models of Gene Regulatory Networks. *Math. Model. Nat. Phenom.*, 3(2), 85–97. Retrieved from <https://doi.org/10.1051/mmnp:2008056>
- Shuen, W. H., Kan, R., Yu, Z., Lung, H. L., & Lung, M. L. (2015). Novel lentiviral-inducible transgene expression systems and versatile single-plasmid reporters for in vitro and in vivo cancer biology studies. *Cancer Gene Therapy*, 22(4), 207–214. doi: 10.1038/cgt.2015.9
- Sprinzak, D., Lakhanpal, A., Lebon, L., Santat, L. A., Fontes, M. E., Anderson, G. A., ...

- Elowitz, M. B. (2010, 5). Cis-interactions between Notch and Delta generate mutually exclusive signalling states. *Nature*, 465(7294), 86–90. Retrieved from <https://www.nature.com/articles/nature08959> doi: 10.1038/nature08959
- Stamatakis, M., & Mantzaris, N. V. (2009). Comparison of Deterministic and Stochastic Models of the lac Operon Genetic Network. *Biophysical Journal*, 96(3), 887–906. Retrieved from <https://www.sciencedirect.com/science/article/pii/S0006349508001008> doi: <https://doi.org/10.1016/j.bpj.2008.10.028>
- Stone, A. V., Vanderman, K. S., Willey, J. S., David, L., Register, T. C., Shively, C. A., ... Ferguson, C. M. (2014). Generation of mouse models of myeloid malignancy with combinatorial genetic lesions using CRISPR-Cas9 genome editing. *Nature Biotechnology*, 32(10), 941–946. doi: 10.1038/nbt.2951
- Stothard, P. (2000). Internet On-Ramp Internet On-Ramp. *BioTechniques*, 28(6), 1102–1104.
- Waterloo. (2022). *CRISPRi*.
- Weinberg, B. H., Pham, N. T., Caraballo, L. D., Lozanoski, T., Engel, A., Bhatia, S., & Wong, W. W. (2017, 5). Large-scale design of robust genetic circuits with multiple inputs and outputs for mammalian cells. *Nature Biotechnology*, 35(5), 453–462. Retrieved from <https://www.nature.com/articles/nbt.3805> doi: 10.1038/nbt.3805
- Yeo, N. C., Chavez, A., Lance-byrne, A., Chan, Y., Milanova, D., Kuo, C.-c., ... Nathan, E. (2019). An enhanced CRISPR repressor for targeted mammalian gene regulation. *Nat Methods*, 15(8), 611–616. doi: 10.1038/s41592-018-0048-5
- Zhou, J., Zhang, Q., Henriquez, J. E., Crawford, R. B., & Kaminski, N. E. (2018, 10). Lymphocyte-Specific Protein Tyrosine Kinase (LCK) is Involved in the Aryl Hydrocarbon Receptor-Mediated Impairment of Immunoglobulin Secretion in Human Primary B Cells. *Toxicological Sciences*, 165(2), 322–334. Retrieved from https://www.researchgate.net/publication/325575258_Lymphocyte-specific_protein_tyrosine_kinase_LCK_is_involved_in_the_aryl_hydrocarbon_receptor_AHR-mediated_impairment_of_immunoglobulin_secretion_in_human_primary_B_cells doi: 10.1093/toxsci/kfy133

Appendix

Model Design

SimBio Model

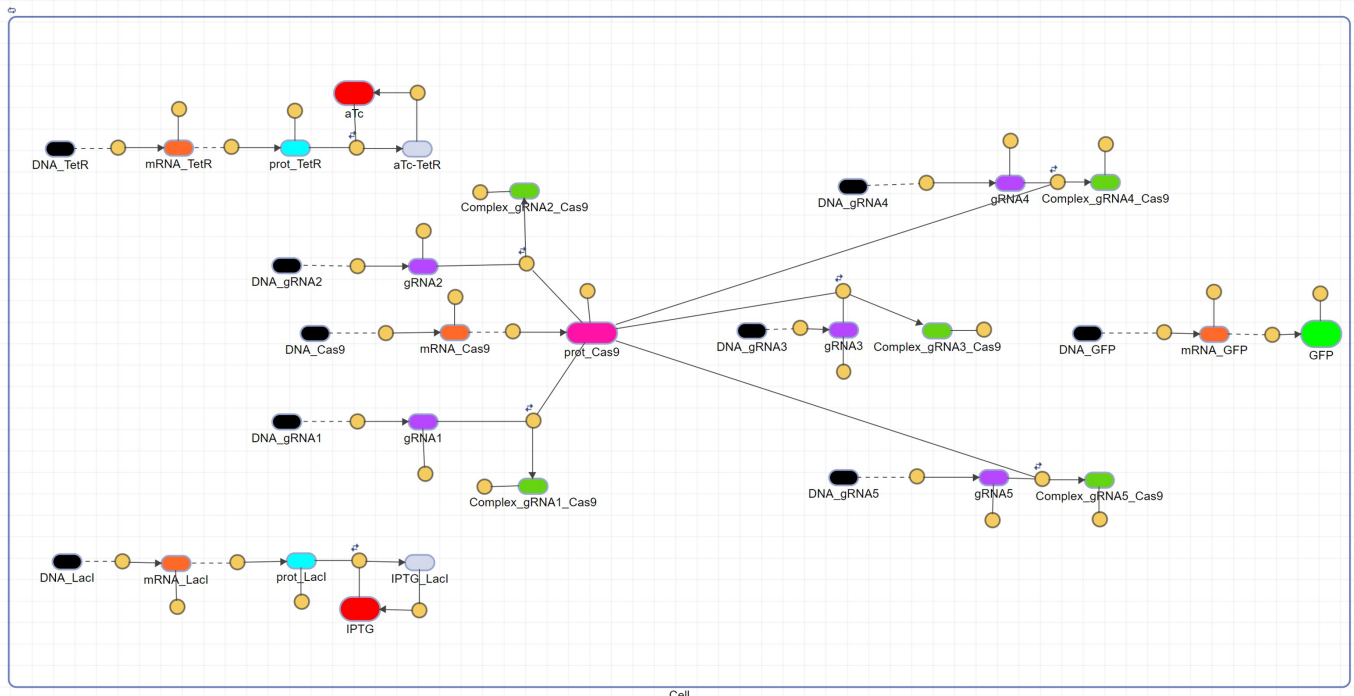


Figure F7: Model network was created by using Simbiology in Matlab. (Red) Input IPTG & Anhydro Tetracycline (aTc). (Black) DNA of each circuit. (Orange) mRNA. (Violet) Guide-RNA (gRNA). (Light blue) Repressor proteins TetR & LacI. (Pink) Cas9 protein. (Green) gRNA recruited Cas9 complex. (Light green) GFP. (Yellow) reactions.

Parameters

Parameter	Value	Unit
Transcription LacI/TetR	0.005	1/second
Translation LacI/TetR	0.015	1/second
Transcription dCas9	0.005	1/second
Translation dCas9	0.015	1/second
Transcription GFP	0.005	1/second
Translation GFP	0.015	1/second
mRNA/gRNA degradation	$2.31 * 10^{-4}$	1/second
Protein degradation	$2.75 * 10^{-5}$	1/second
k_{on} IPTG/aTc + LacI/TetR	1.66e-4	1/(molecule*second)
k_{off} IPTG/aTc + LacI/TetR	1.93e-4	1/second
K_d LacI/TetR + LacO/TetO	60.22	molecule
Transcription gRNA	0.02	1/second
k_{on} gRNA + Cas9	1.66e-5	1/(molecule*second)
k_{off} gRNA + Cas9	10^{-5}	1/second
K_d gRNA-Cas9 + target	16.8	molecule
Hill coefficient	2.5	-

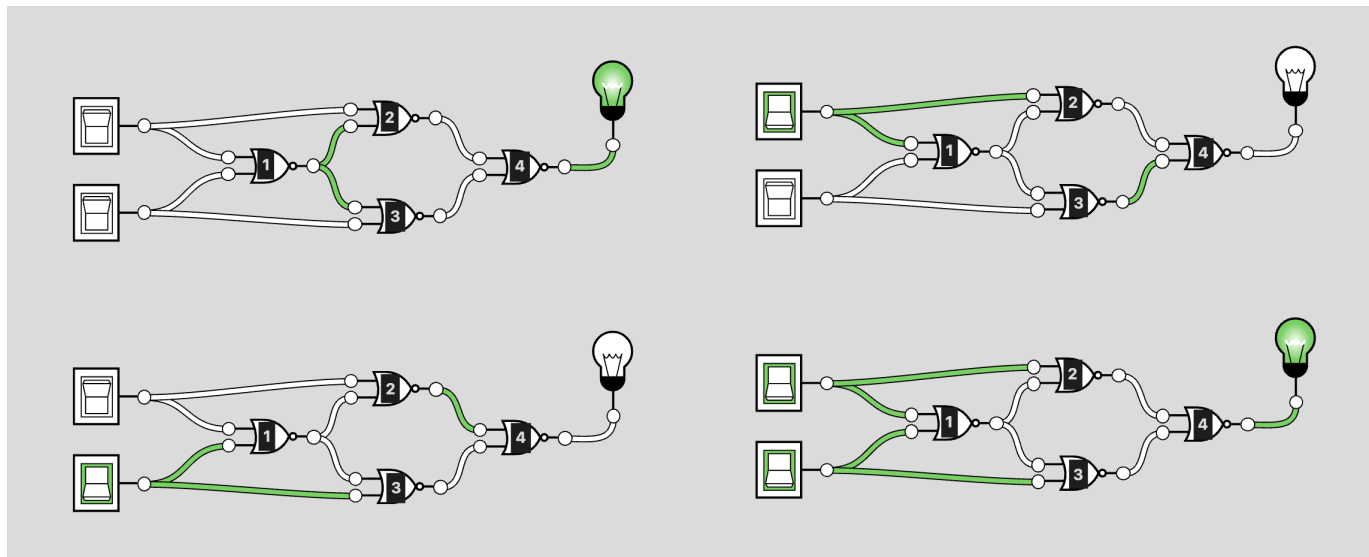


Figure F8: Graphical simulation of XNOR gate function for all different inputs. Green colouring signifies a positive output.

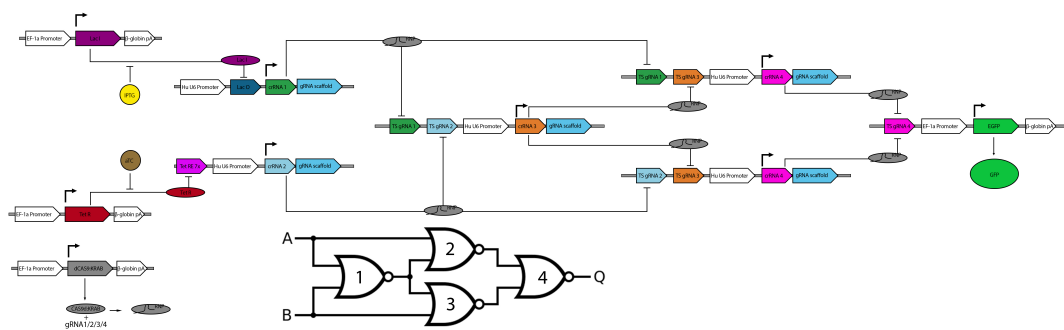
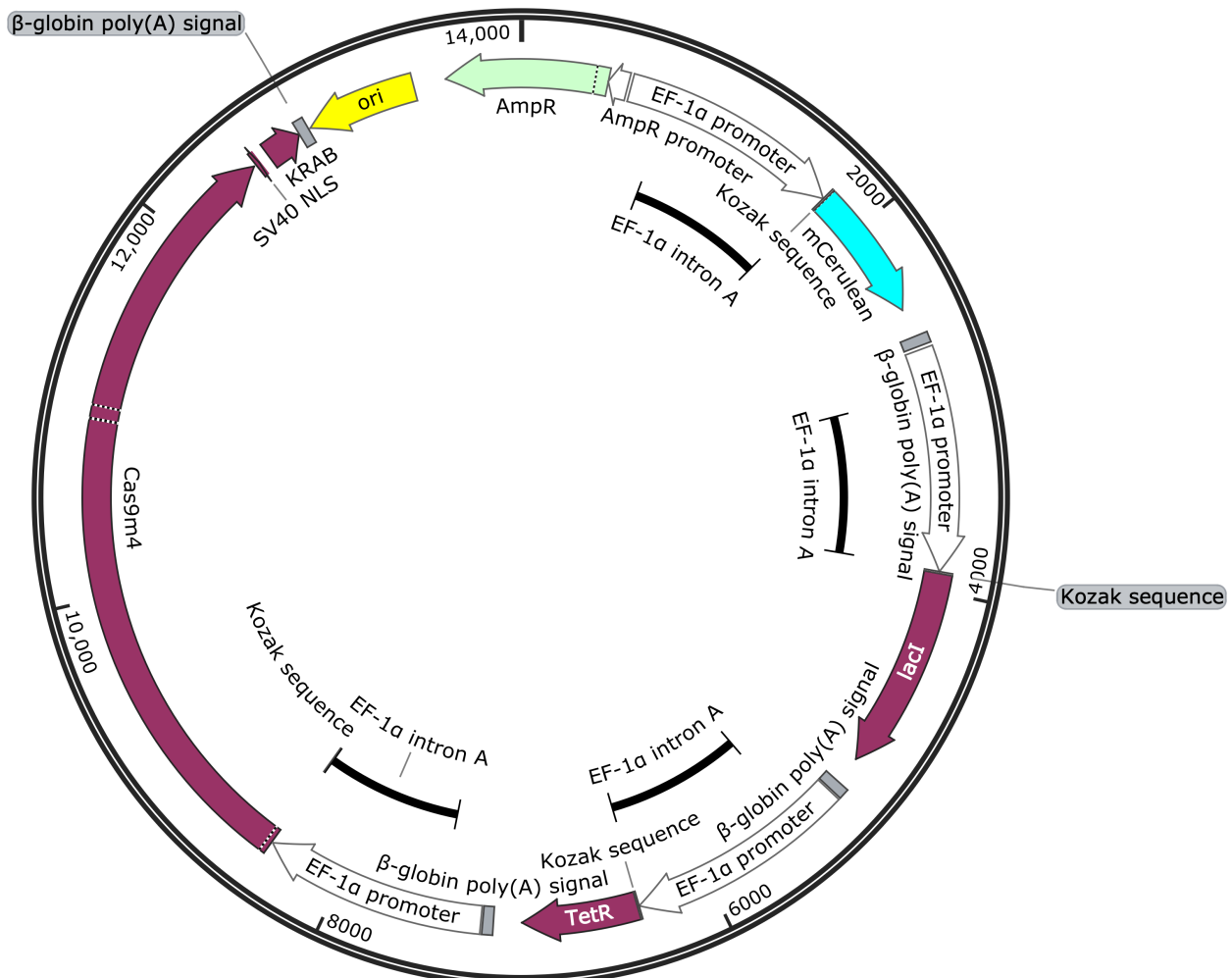


Figure F10: Overview of the system design. Each component as described in section construct design and system design is depicted as a simplified summary of the respective DNA sequences as available in the online depository. A full resolution file of the graphic is available [online](#).



EF1-a_Cerulean_EF1-a_LacI_EF1-a_TetR_EF1-a_dCAS9_KRAB_AmpR
14,032 bp

Figure F11: Sequence map of expression plasmid 001 pBC001. pBC001 contains the expression cassettes for mCerulean, LacI, TetR, dCas9-KRAB and the Ampicillin resistance. The plasmids total size is 14kb.

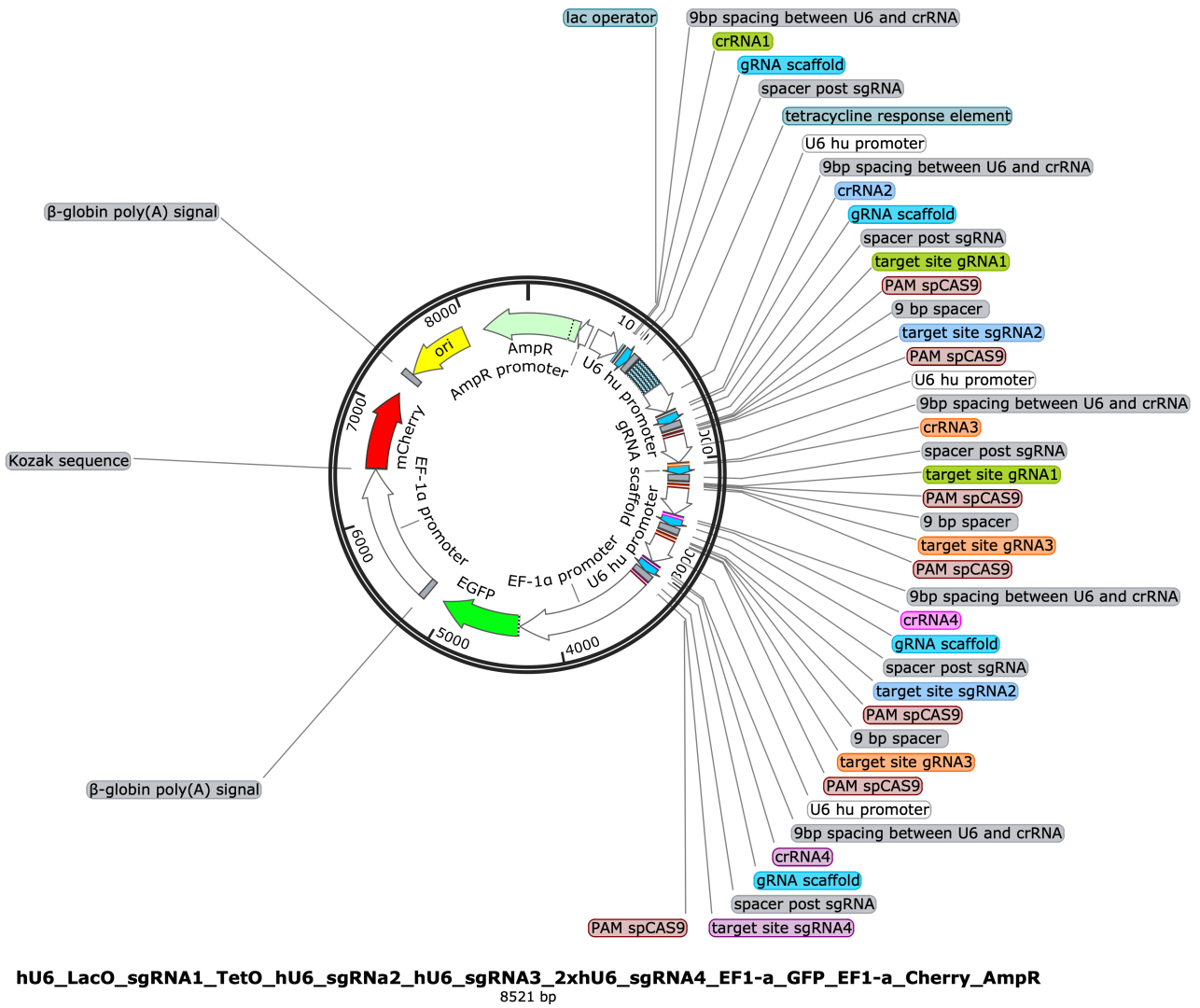


Figure F12: Sequence map of expression plasmid 002 pBC002. pBC002 contains the expression cassettes for sgRNA1-sgRNA4 as well as their respective regulatory sites controlling each cassette's human U6 promoter. The plasmid also contains the GFP, mCherry and Ampicillin resistance expression cassettes. The plasmid's total size is 8.5kb.